A Quantitative Model of the Switch Cycle of an Archaeal Flagellar Motor and its Sensory Control

Torsten Nutsch,* Dieter Oesterhelt,† Ernst Dieter Gilles,* and Wolfgang Marwan‡
*Max-Planck-Institute for Dynamics of Complex Technical Systems, Magdeburg, Germany; †Max-Planck-Institute for Biochemistry, Martinsried, Germany; and ‡Science and Technology Research Institute, University of Hertfordshire, Hatfield, United Kingdom

ABSTRACT By reverse-engineering we have detected eight kinetic phases of the symmetric switch cycle of the *Halobacterium salinarum* flagellar motor assembly and identified those steps in the switch cycle that are controlled by sensory rhodopsins during phototaxis. Upon switching the rotational sense, the flagellar motor assembly passes through a stop state from which all subunits synchronously resume rotation in the reverse direction. The assembly then synchronously proceeds through three subsequent functional states of the switch: Refractory, Competent, and Active, from which the rotational sense is switched again. Sensory control of the symmetric switch cycle occurs at two steps in each rotational sense by inversely regulating the probabilities for a change from the Refractory to the Competent and from Competent to the Active rotational mode. We provide a mathematical model for flagellar motor switching and its sensory control, which is able to explain all tested experimental results on spontaneous and light-controlled motor switching, and give a mechanistic explanation based on synchronous conformational transitions of the subunits of the switch complex after reversible dissociation and binding of a response regulator (CheYP). We conclude that the kinetic mechanism of flagellar motor switching and its sensory control is fundamentally different in the archaeon *H. salinarum* and the bacterium *Escherichia coli*.

INTRODUCTION

Halobacterium salinarum cells are rod-shaped archaea that have developed a sophisticated system for sensing and response, mediating adaptation to a wide variety of environmental conditions by regulating gene expression and motility (note that, during the years, the name of this species was changed from *Halobacterium halobium* to *H. salinarium*, then to *H. salinarum*). The cellular swimming behavior is controlled by numerous chemical and physical stimuli that are sensed and processed by a fine-tuned regulatory network enabling the cells to accumulate at those sites of their extreme habitat that provide the best combination of conditions available at the moment. Of 18 genomically encoded methyl-accepting halobacterial transducer proteins (Htr) (Halolex database at http://www.halolex.mpg.de), eight were shown to act as specific sensors and/or transducers for light, amino acids, compatible solutes, oxygen, and proton motive force (1), feeding into a two-component system that integrates the sensory input to regulate the swimming behavior of the cell. Many elements of the halobacterial Htr-dependent two-component system, CheA, CheB, CheC, CheD, CheJ, CheJ2, CheJ3, CheR, CheW1, CheW2, and CheY are orthologs of the correspondingly named bacterial chemotaxis proteins (2), though the halobacterial system is composed of more elements than the *Escherichia coli* chemotaxis machinery and in this respect is reminiscent to *Bacillus subtilis* (3 and references therein). The histidine kinase CheA phosphorylates the response regulator CheY, which in a phosphorylated form interacts with the flagellar motor.

Halobacteria can grow phototrophically with the help of two retinal-containing light-driven ion pumps, bacteriorhodopsin and halorhodopsin, which generate proton motive force for ATP synthesis and mediate chloride uptake during growth (4). Two additional retinal proteins, sensory rhodopsin I (SRI) and SRII, are specifically complexed with their cognate transducer proteins (HtrI and HtrII) and mediate phototaxis to guide the cells to the light conditions optimal for phototrophic growth (5). Bacteriorhodopsin, halorhodopsin, and the two sensory rhodopsins form a family of closely related seven-helix transmembrane proteins. The mechanism of photoactivation in all four rhodopsins is similar. Light photoisomerizes the covalently bound all-*trans* retinal to 13-*cis*, which then re-isomerizes to all-*trans* in a light-independent reaction. In the pumps, this photocycle drives the light-energy-converting ion translocation across the membrane. In the sensory rhodopsins, isomerization of retinal by the light signal is conformationally coupled to the signaling domain of the transducer proteins (5–7).

Although the protein network mediating photo- and chemotaxis in *Halobacterium* is similar to the bacterial counterpart, its target, the archaeal flagellar motor apparatus is built from a completely different set of proteins than the bacterial flagellar motor: In none of the archaeal genomes sequenced so far have orthologs of the bacterial flagellar motor components been found (8,9). Hence the archaeal flagellar motor and the bacterial flagellar motor are organelles

Submitted December 5, 2004, and accepted for publication May 17, 2005.

Torsten Nutsch's present address is ZF Lenksysteme, Richard-Bullinger-Straße, 73527 Schwäbisch Gmünd, Germany.

Address reprint requests to Wolfgang Marwan, Max-Planck-Institute for Dynamics of Complex Technical Systems and Institute for Biology, Otto-von-Guericke-University Magdeburg, Sandtorstrasse 1, 39106 Magdeburg, Germany. Tel.: 49-6110-410; E-mail: marwan@mpi-magdeburg.mpg.de.

0006-3495/05/10/2307/17 $2.00

doi: 10.1529/biophysj.104.057570

of different evolutionary origin and possibly operate with a fundamentally different mechanism.

H. salinarum cells swim by means of a polarly inserted flagellar bundle composed of 5–10 flagellar filaments that associate to form a semirigid right-handed helical superstructure (10). The flagellar bundle propels the cells by a rotary mechanism. When a cell is tethered by immobilizing the bundle on a solid surface, the cell spins—alternating between clockwise and counterclockwise directions, depending on the rotational sense of the flagellar motors (10). Spinning of tethered cells is the classical evidence for the rotary mechanism of the bacterial flagellar motor (11). The halobacterial flagellar bundle works as a functional unit (see below), but whether each of its flagellar filaments is powered by an individual flagellar motor is not yet established. However, in *Haloarcula quadrata*, a related species, flagellar filaments emerging from different sites of the cell surface merge to form a rotating flagellar bundle. When this bundle is tethered, the cell spins without winding the bundle up, indicating that the filaments glide along each other while being powered by spatially separated motors (12).

H. salinarum cells swim back and forth by rotating the flagellar bundle clockwise (CW) or counterclockwise (CCW). Unstimulated cells spontaneously switch the rotational sense from time to time performing a random walk. Light and other sensory stimuli bias the random walk with respect to the stimulus source. Attractant stimuli suppress spontaneous switching, allowing the cell to continue swimming in the favorable direction. Repellent stimuli, however, induce motor switching, which makes the cell reverse its path and flee the stimulus source. Orange light is an attractant, whereas blue- and UV-light are repellents (see Ref. 1 and references therein).

Cells are equally sensitive to stimulation in each rotational sense (13). After a cell has been exposed to a repellent light stimulus, it continues to swim with constant speed until it suddenly stops and reverses its swimming direction by switching the rotational sense of the flagellar motor assembly (14). The stop typically takes up to several hundred milliseconds. The length of the stop phase may change from reversal to reversal in the same cell, suggesting that the transitions from rotation to stop and from stop to reverse rotation occur stochastically (14). Since cells swim with constant speed before entering the stop phase, individual flagellar motors do not seem to switch the rotational sense independently. The mechanism of synchronization is not known, but obviously the flagellar motor assembly acts as a functional unit in rotation and switching (14). As a switch complex, we therefore define the protein components of the flagellar motors that determine the rotational sense in a coordinated way.

Here we show that the switch complex proceeds through a sequence of kinetically resolved functional states some of which are susceptible to sensory control. We present a mechanistic model for switching of the rotational sense of the archaeal flagellar motor, and by coupling it to a kinetic model of the signaling pathway we provide the first coherent model of archaeal sensing and response, which is able to reproduce all experimental results tested so far.

METHODS

The refined kinetic model for motor switching was implemented by solving a set of ordinary differential equations in MatLab (The MathWorks, Natick, MA) as follows. Starting from the Petri Net model (Model 3) a detailed dynamic kinetic model was implemented. Experiments show that the switch mechanism behaves identically in both swimming directions. Therefore the model had to consider one rotational sense only. It is assumed that each of the $n_s = 44$ subunits of the switch complex can bind CheYP and is responsible for activating the reversal process. The switch complex as a whole can be in one of the phases as shown in the Petri Net of Fig. 2 (*Refractory*, *R*; *Competent*, *C*; *Active*, *A;* or *Stop*, *S*). The state variables represent the probability of the complex to be in a certain phase and to be complexed with *i* CheYP molecules:

$$\begin{aligned} &R_i; \quad i \in [0 \ldots 44], \\ &C_i; \quad i \in [0 \ldots 44], \\ &A_j; \quad j \in [0 \ldots 43], \\ &S. \end{aligned}$$

During the Active phase, each subunit undergoes a modification reaction, e.g., a conformational change. The state of the modification is indicated by the superscript *k*. For simplicity, it is assumed that, during the Active and the Stop phases, the occupancy level *i* of the complex stays constant. Otherwise the number of states to be considered by computation would have been tremendously high. The association and dissociation reactions during the Refractory and Competent phases are assumed to occur in parallel. Thus the

TABLE 1 Model parameters

Parameter	Value	Description
k_{assR}	0.5341 $[CheYP_{ss}]^{-1}$ s^{-1}	Association rate constant of CheYP to subunits during the Refractory phase.
k_{dissR}	0.9314 s^{-1}	Dissociation rate constant of CheYP from subunits during the Refractory phase.
k_1^0	0.8100×10^6 s^{-1}	Pre-exponential factor for the transition of Refractory to Competent.
R	0.6	Exponential factor for the transition of Refractory to Competent.
k_{assC}	0.1177 $[CheYP_{ss}]^{-1}$ s^{-1}	Association rate constant of CheYP to subunits during the Competent phase.
k_{dissC}	0.03338 s^{-1}	Dissociation rate constant of CheYP from subunits during the Competent phase.
k_2^0	2.07×10^{-9} s^{-1}	Pre-exponential factor for the transition of Competent to Active.
C	0.6	Exponential factor for the transition of Competent to Active.
k_s	7 s^{-1}	Rate constant of conformational changes in subunits during the Active phase.
k_{stop}	2.48 s^{-1}	Transition rate constant of Stop to Refractory phases.

number of binding sites that are still free has to be taken into account for each individual step. During the refractory phase, the following individual steps occur:

$$\begin{aligned} \mathrm{CheYP} + R_\mathrm{i} &\xrightarrow{(44-i)\cdot k_\mathrm{assR}} R_{\mathrm{i}+1}; \quad i \in [0 \ldots 43], \\ R_\mathrm{i} &\xrightarrow{i\cdot k_\mathrm{dissR}} R_{\mathrm{i}-1} + \mathrm{CheY} + \mathrm{P_i}; \quad i \in [1 \ldots 44], \\ R_\mathrm{i} &\xrightarrow{k_\mathrm{i}^0 \cdot e^{-\mathrm{i}\cdot\mathrm{R}}} C_\mathrm{i}; \quad i \in [0 \ldots 44]. \end{aligned}$$

Thereby it is assumed that with decreasing occupancy of the complex the probability for a transition to the Competent phase increases. Accordingly, the behaviour of the switch complexes in the Refractory phase was described by a set of 44 differential equations, describing the reactions of each of the 44 subunits of a switch complex independently from the other 43 subunits:

$$\begin{aligned} \frac{d[R_0]}{dt} &= k_\mathrm{dissR}\cdot[R_1] \\ &\quad - 44\cdot k_\mathrm{assR}\cdot[CheYP]\cdot[R_0] - k_1^0\cdot[R_0], \\ \frac{d[R_\mathrm{i}]}{dt} &= (44-i+1)\cdot k_\mathrm{assR}\cdot[CheYP]\cdot[R_{\mathrm{i}-1}] + (i+1)\cdot \\ &\quad k_\mathrm{dissR}\cdot[R_{\mathrm{i}+1}] - (44-i)\cdot k_\mathrm{assR}\cdot[CheYP]\cdot[R_\mathrm{i}] \\ &\quad - i\cdot k_\mathrm{dissR}\cdot[R_\mathrm{i}] - k_1^0\cdot e^{-\mathrm{i}\cdot\mathrm{R}}\cdot[R_\mathrm{i}]; \quad i \in [1..43], \\ \frac{d[R_{44}]}{dt} &= k_\mathrm{assR}\cdot[CheYP]\cdot[R_{43}] \\ &\quad - 44\cdot k_\mathrm{dissR}\cdot[R_{44}] - k_1^0\cdot e^{-44\cdot\mathrm{R}}\cdot[R_{44}]. \end{aligned}$$

Each differential equation describes, within a large population of switch complexes, the concentration of those switch complexes that are in the Refractory phase and that have *i* CheYP molecules bound. Hence, a statistical distribution displaying the relative abundance of switch complexes in the Refractory phase that have 0, 1, 2–44 CheYP molecules bound, can be determined for any selected time-point by evaluating the set of 44 kinetic curves.

During the Competent phase the following reactions occur:

$$\begin{aligned} \mathrm{CheYP} + C_\mathrm{i} &\xrightarrow{(44-i)\cdot k_\mathrm{assC}} C_{\mathrm{i}+1}; \quad i \in [0 \ldots 43], \\ C_\mathrm{i} &\xrightarrow{i\cdot k_\mathrm{dissC}} C_{\mathrm{i}-1} + \mathrm{CheY} + \mathrm{P_i}; \quad i \in [1 \ldots 44], \\ C_\mathrm{i} &\xrightarrow{k_2^0\cdot e^{+\mathrm{i}\cdot\mathrm{C}}} A^0; \quad i \in [0 \ldots 44]. \end{aligned}$$

These are again described by a set of 44 differential equations, according to

$$\begin{aligned} \frac{d[C_0]}{dt} &= k_\mathrm{dissC}\cdot[C_1] \\ &\quad - 44\cdot k_\mathrm{assC}\cdot[CheYP]\cdot[C_0] + k_1^0\cdot[R_0] - k_2^0\cdot[C_0], \\ \frac{d[C_\mathrm{i}]}{dt} &= (44-i+1)\cdot k_\mathrm{assC}\cdot[CheYP]\cdot[C_{\mathrm{i}-1}] + (i+1)\cdot k_\mathrm{dissC}\cdot \\ &\quad [C_{\mathrm{i}+1}] - (44-i)\cdot k_\mathrm{assC}\cdot[CheYP]\cdot[C_\mathrm{i}] - i\cdot k_\mathrm{dissC}\cdot \\ &\quad [C_\mathrm{i}] + k_1^0\cdot e^{-\mathrm{i}\cdot\mathrm{R}}\cdot[R_\mathrm{i}] - k_2^0\cdot e^{+\mathrm{i}\cdot\mathrm{C}}\cdot[C_\mathrm{i}]; \quad i \in [1..43], \\ \frac{d[C_{44}]}{dt} &= k_\mathrm{assC}\cdot[CheYP]\cdot[C_{43}] - 44\cdot k_\mathrm{dissC}\cdot[C_{44}] \\ &\quad + k_1^0\cdot e^{-44\cdot\mathrm{R}}\cdot[R_{44}] - k_2^0\cdot e^{+44\cdot\mathrm{C}}\cdot[C_{44}]. \end{aligned}$$

In the Active phase, the individual subunits react in parallel as well,

$$A^\mathrm{j} \xrightarrow{(44-j)\cdot k_\mathrm{s}} A^{\mathrm{j}+1}; \quad j \in [0 \ldots 42].$$

The final reaction step in the Active phase generates the Stop state,

$$A^{43} \xrightarrow{k_\mathrm{s}} S,$$

resulting in the time-dependent equations of the Active phase,

$$\begin{aligned} \frac{d[A^0]}{dt} &= -44\cdot k_\mathrm{s}\cdot[A^0] + \sum_{\mathrm{i}=0}^{44} k_2^0\cdot e^{\mathrm{i}\cdot\mathrm{C}}\cdot[C_\mathrm{i}]; \\ \frac{d[A^\mathrm{j}]}{dt} &= -(44-j)\cdot k_\mathrm{s}\cdot[A^\mathrm{j}] + (44-j+1)\cdot \\ &\quad k_\mathrm{s}\cdot[A^{\mathrm{j}-1}]; \quad j \in [1 \ldots 43]. \end{aligned}$$

Finally the flagellar motor resumes rotation in the opposite rotational sense according to a first-order reaction,

$$S \xrightarrow{k_\mathrm{stop}} \text{reversal},$$

resulting in a time-dependent change in the switch complexes that are in the Stop phase as

$$\frac{d[S]}{dt} = k_\mathrm{s}\cdot[A^{43}] - k_\mathrm{stop}\cdot[S].$$

Experiments with asynchronous cells

When cells are picked at random, i.e., without knowing when the flagellar motor performed its last reversal, each subsequent reversal of a cell is counted (perhaps several times, depending on the type of experiment) to calculate the reversal frequency. In this case, the final reversal completes the switching cycle. For simplicity, it is assumed that the occupancy level of the switching complex is not influenced during the Active and Stop phases:

$$S \xrightarrow{k_\mathrm{rev,i}} R_\mathrm{i}; \quad i \in [0 \ldots 44].$$

Consequently, the rate $r_\mathrm{rev,i} = [S]\cdot k_\mathrm{rev,i}$ is approximated by

$$r_\mathrm{rev,i} = [S]\cdot k_\mathrm{stop}\frac{[C_\mathrm{i}]\cdot e^{+\mathrm{i}\cdot\mathrm{C}}}{\sum_{\mathrm{j}=0}^{44}[C_\mathrm{j}]\cdot e^{+\mathrm{j}\cdot\mathrm{C}}}.$$

Since in asynchronous cell populations there are always at least some switch complexes in the Competent phase, the denominator is always >0. The differential equations given above describe the behavior of the switch complexes in the Refractory phase only, if one motor switching event is to be simulated. If, in contrast, successive motor switching events are simulated, the occupancy level of the subunits contributed from switch complexes that have been in the Stop phase are to be considered in addition. The set of differential equation then reads

$$\begin{aligned} \frac{d[R_0]}{dt} &= k_\mathrm{dissR}\cdot[R_1] - 44\cdot k_\mathrm{assR}\cdot[CheYP]\cdot[R_0] \\ &\quad - k_1^0\cdot[R_0] + [S]\cdot k_\mathrm{stop}\frac{[C_0]}{\sum_{\mathrm{j}=0}^{44}[C_\mathrm{j}]\cdot e^{+\mathrm{j}\cdot\mathrm{C}}}, \\ \frac{d[R_\mathrm{i}]}{dt} &= (44-i+1)\cdot k_\mathrm{assR}\cdot[CheYP]\cdot[R_{\mathrm{i}-1}] + (i+1)\cdot \\ &\quad k_\mathrm{dissR}\cdot[R_{\mathrm{i}+1}] - (44-i)\cdot k_\mathrm{assR}\cdot[CheYP]\cdot[R_\mathrm{i}] - i\cdot k_\mathrm{dissR}\cdot \\ &\quad [R_\mathrm{i}] - k_1^0\cdot e^{-\mathrm{i}\cdot\mathrm{R}}\cdot[R_\mathrm{i}] + [S]\cdot k_\mathrm{stop}\frac{[C_\mathrm{i}]\cdot e^{+\mathrm{i}\cdot\mathrm{C}}}{\sum_{\mathrm{j}=0}^{44}[C_\mathrm{j}]\cdot e^{+\mathrm{j}\cdot\mathrm{C}}}, \quad i \in [1..43] \end{aligned}$$

$$\frac{d[R_{44}]}{dt} = k_{\mathrm{assR}} \cdot [CheYP] \cdot [R_{43}] - 44 \cdot k_{\mathrm{dissR}} \cdot [R_{44}] - k_1^0 \cdot e^{-44 \cdot \mathrm{R}} \cdot [R_{44}] + [S] \cdot k_{\mathrm{stop}} \frac{[C_{44}] \cdot e^{+44 \cdot \mathrm{C}}}{\sum_{\mathrm{j}=0}^{44} [C_{\mathrm{j}}] \cdot e^{+\mathrm{j} \cdot \mathrm{C}}}.$$

Experiments with synchronous cells

When experiments were simulated, where the time of the last reversal was known, the initial distribution of the occupancy level directly after this last reversal had to be determined first. Therefore successive simulations were performed where the final distribution in the Competent phase served as initial distribution of the Refractory phase for the next simulation. After few repetitions the distribution reaches a steady state.

The probability density function of interval lengths (reversals per time interval) can be calculated from the first passage time of the process. Because stopping of the cells was interpreted as the end of a swimming interval by the experimentalists, the last step of the Active phase determines the reversal probability density function:

$$P_{\mathrm{reversal}}(t) = [A^{43}](t) \cdot k_{\mathrm{s}}.$$

Signal transduction

For the adaptational mechanism only a very simple model has been used, making as few assumptions as possible. Depending on the experiment, either the model of SRI or the model of SRII has been used (not both at the same time). Both receptors are modeled with three states.

SRI

$$SR_{587} \xrightarrow{I_{\mathrm{or}} \cdot \sigma\phi} SR_{373}$$
$$SR_{373} \xrightarrow{I_{\mathrm{UV}} \cdot \sigma\phi} SR_{510}$$
$$SR_{373} \xrightarrow{k_{\mathrm{r373}}} SR_{587}$$
$$SR_{510} \xrightarrow{k_{\mathrm{r510}}} SR_{587}$$
$$[SR_{587}] + [SR_{373}] + [SR_{510}] = 1,$$

SRII

$$SR_{487} \xrightarrow{I_{\mathrm{bl}} \cdot \sigma\phi} SR_{360}$$
$$SR_{360} \xrightarrow{k_{\mathrm{r360}}} SR_{540}$$
$$SR_{540} \xrightarrow{k_{\mathrm{r540}}} SR_{487}$$
$$[SR_{487}] + [SR_{360}] + [SR_{540}] = 1,$$

where I_{or}, I_{uv}, and I_{bl} are the orange-, UV-, and blue-light intensities, respectively. The parameter σ denotes the photon-activatable area of a receptor, and ϕ is the photon efficiency.

Methylation

The two methylation states of the transducers are M_0 and M_1. Methylation and demethylation is mediated by CheR and CheBP, respectively; the concentration of CheR is constant. These enzymes are assumed to work at substrate saturation, i.e., the reaction rate is only dependent on the total concentration of the enzyme and does not depend on the concentration of substrate. The equations for M_0 and M_1 are

$$\frac{d[M_1]}{dt} = k_{\mathrm{meth}} \cdot [M_0] - k_{\mathrm{dem}} \frac{[\mathrm{CheBP}]}{[\mathrm{CheBP_{ss}}]} \cdot [M_1],$$
$$[M_0] = 1\text{-}[\mathrm{M_1}],$$

where $[\mathrm{CheBP_{ss}}]$ is the concentration of CheBP under steady-state conditions.

Activity of the sensory rhodopsin transducer complexes

Finally, each combination of methylation and receptor state is assigned a specific level of activity and the mean activity A can be calculated by

SRI

$$A = [SR_{587}]([M_0]\alpha_{587\mathrm{M0}} + [M_1]\alpha_{587\mathrm{M1}}) + [SR_{373}]([M_0]\alpha_{373\mathrm{M0}} + [M_1]\alpha_{373\mathrm{M1}}) + [SR_{510}]([M_0]\alpha_{510\mathrm{M0}} + [M_1]\alpha_{510\mathrm{M1}}).$$

SRII

$$A = [SR_{487}]([M_0]\alpha_{487\mathrm{M0}} + [M_1]\alpha_{487\mathrm{M1}}) + [SR_{360}]([M_0]\alpha_{360\mathrm{M0}} + [M_1]\alpha_{360\mathrm{M1}}) + [SR_{540}]([M_0]\alpha_{540\mathrm{M0}} + [M_1]\alpha_{540\mathrm{M1}}).$$

CheYP

The activity level of the receptors determines the level of CheYP and CheBP concentration. The dynamics of phosphotransfer reactions and the nonlinear characteristic is thereby neglected,

$$\frac{[\mathrm{CheYP}]}{[\mathrm{CheYP_{ss}}]} = \begin{cases} 0 & ; A \le 0 \\ A & ; 0 < A < y_{\max} \\ y_{\max} & ; A \ge y_{\max}, \end{cases}$$
$$\frac{[\mathrm{CheBP}]}{[\mathrm{CheBP_{ss}}]} = \begin{cases} 0 & ; A \le 0 \\ A & ; 0 < A < b_{\max} \\ b_{\max} & ; A \ge b_{\max}, \end{cases}$$

where A is the mean activity of the sensory rhodopsin transducer complex. Kinetic parameter values for the sensory rhodopsins and for the signaling pathway are given in Table 2.

RESULTS

The mechanistic model for flagellar motor switching in *H. salinarum*, as presented in its final form in this work, reflects a set of intrinsic properties of the switch complex. We aim to show how each single feature of the model is derived from an experimentally determined functional property of the flagellar motor switch. Consequently, we will develop the model step by step, starting from the most simple two-state model

TABLE 2 Model parameters for the sensory rhodopsins and the signaling pathway

SRI			SRII		
$\sigma\phi$	1.47×10^{-20}	m^2	$\sigma\phi$	1.47×10^{-20}	m^2
$k_{r\ 373}$	0.924	1/s	$k_{r\ 360}$	0.577	1/s
$k_{r\ 510}$	8.66	1/s	$k_{r\ 540}$	0.21	1/s
$\alpha_{587M\ 0}$	0		$\alpha_{487M\ 0}$	−0.6	
$\alpha_{587M\ 1}$	30		$\alpha_{487M\ 1}$	1.1	
$\alpha_{370M\ 0}$	−2.04		$\alpha_{360M\ 0}$	0	
$\alpha_{370M\ 1}$	1.1		$\alpha_{360M\ 1}$	250	
$\alpha_{510M\ 0}$	1		$\alpha_{540M\ 0}$	0	
$\alpha_{510M\ 1}$	518		$\alpha_{540M\ 1}$	250	
Methylation					
k_{meth}	0.0212	1/s	y_{max}	30	
k_{dem}	0.0212	1/s	b_{max}	3	

and introducing new elements whenever necessary to account for experimental results. Although the kinetic model finally derived will appear quite complex at the first glance, it will become obvious that only a few assumptions were incorporated and that these assumptions have predictive value. The validity of the general model structure (Model *3*) however, holds independent of the assumptions made. We use the Petri Net formalism to represent the models for the switch complex. The Petri Net theory provides a simple, intuitively understandable language of description with a qualitative graphical representation of the network structure and dynamics, able to consistently describe processes of highly different complexity within a single, coherent model. The Petri Net theory provides mathematically proven methods and there are numerous implemented tools, most of them freely available (15–18).

The Petri Net formalism has three elements—places, transitions, and tokens. Upon the switching of a transition, a token moves from place *a* to place *b*. The formalism allows places or transitions to be refined into subnetworks, describing individual biochemical reactions (19–26), while other parts of the same model may still represent complex processes not yet resolved down to the molecular level. In other words, any biochemical reaction can be represented as a Petri Net; however, a Petri Net can also simultaneously operate at the molecular or higher levels of description. In addition, dependent on the number of tokens used, it permits us to switch between deterministic and stochastic descriptions within the same model structure, or to couple stochastic and deterministic steps of a given pathway. This is especially helpful for the analysis of such biochemical networks, where single molecules or photons are able to cause a biological effect.

First, we will describe simple Petri Net models for the switch complex (Models *1–3*), qualitatively accounting for the functional states of the flagellar motor assembly as derived from behavioral experiments (a brief introduction to Petri Nets is given below). Second, we will estimate the kinetic properties of each functional state assuming multiple subunits of the switch complex to bind the switching signal (that is, CheYP; note that it is assumed that only the phosphorylated response regulator CheYP is the active form and can bind to the switch complex) in a simplified way. Third, all properties are then merged into a final and detailed kinetic model (Model *5*). This kinetic model is able to quantitatively reproduce the results from all types of experiments tested, and explains even those results that are counterintuitive.

Petri Net models of the switch complex

For the sake of simplicity and consistency in description, we choose a hierarchical stochastic Petri Net representation (16,17) of the functional states of the flagellar motor assembly because this model type formally allows refinements of the model structure by resolving individual model components into subnetworks, leaving the precursor model valid and mathematically correct. A short introduction to the Petri Net formalism taking halobacterial motor switching as an example is given in the legend to Fig. 1.

Simplest model

Because halobacterial cells switch between CW and CCW rotation of the flagellar bundle, the switch complex can be described by a two-state model, representing both run phases and the transitions between the two phases (Fig. 1 *C*; Model *1*). A place representing CW rotation marked by a token indicates that the flagellar motor assembly is rotating CW. Switching from CW to CCW rotation occurs when the token moves from the P_{Run1} to the P_{Run2} place, which happens only if the transition T_{R12} switches. Since there is only one token in the network, the motor assembly according to the model cannot rotate CW and CCW at the same time. Instead, the model motor will continuously alter between the CW and CCW rotational functional states.

Stop phase

Switching from one rotational sense to the other includes a period of stopping. This is shown in Fig. 1 *A* for a cell responding to a near UV-light repellent stimulus. After perceiving the stimulus, cells continue to swim with constant speed until the flagellar motor suddenly stops for up to several hundred milliseconds (Fig. 1 *B*; see also Ref. 14). After stopping, the cells resume swimming by reverse motor rotation. To account for the Stop phase, the two-state model (Model *1*; Fig. 1 *C*) is refined by resolving transition T_{R12} into T_{RS1} (Transition Run-Stop1), P_{Stop1}, T_{SR2} (Transition Stop-Run2) and T_{R21} into T_{RS2}, P_{Stop2}, T_{SR1} to give the four-state model (Model *2*; Fig. 1 *C*). The network still contains only one token, since the flagellar bundle cannot rotate and stop at the same time. The token continually changes in a cyclic process from CW (P_{Run1}) to Stop (P_{Stop1}) to CCW (P_{Run2}) to Stop to CW and so on, since wild-type cells never stop without switching the rotational sense. Thermodynamically this means that at least one of the transitions must depend on an

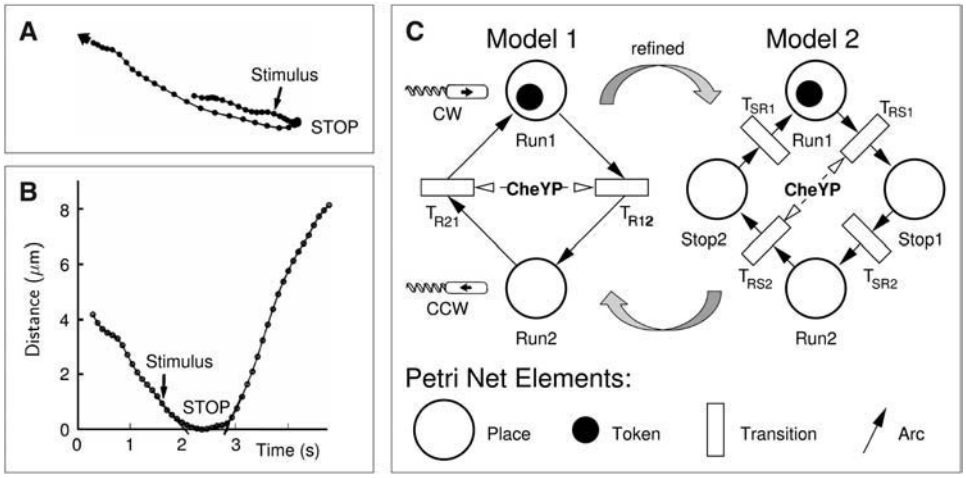

FIGURE 1 (*A*) Typical swimming path of a cell before and after stimulation with a near UV-light pulse, as recorded with a computerized cell tracking system. The positions of the cell centers are plotted with 100-ms time resolution. (*B*) Distance of the position of the cell center from the point of reversal (defined as distance = 0). The curve was calculated using the path shown in *A*. Note that there is some passive displacement of the cell by Brownian motion, which superimposes with the active motion of the cell. Hence the Stop period of the flagellar motor assembly is estimated by extrapolating the falling and the rising flank of the curve to distance = 0. The slight displacement of the cell center during the extrapolated Stop phase is within the tracking error and cannot be regarded as significant. Data for *A* and *B* were taken from Marwan et al. (14). (*C*) Petri Net models of rotation and switching. Petri Nets are bipartite graphs consisting of the elements listed in the figure. Hierarchical Petri Nets, as applied in this study, conceptually allow the resolution of individual places or transitions into a subnetwork, resulting in a refined model. Arrows from CheYP to transitions indicate the influence of CheYP on the transition probability. The thick arrow within the cell symbol indicates the swimming direction.

energy-consuming step. It is neither known at which step(s) of the cycle energy is consumed, nor is there any information on the nature of the energy-consuming reaction. The hydrolysis of the phosphate group of CheYP, e.g., upon dissociation from the subunits in the Refractory phase (see below) of the switch complex seems to be a possible energy-supply. In addition, hydrolysis of CheYP would explain its increased dissociation during the Refractory phase, because unphosphorylated CheY is assumed either not to bind to the switch complex, or to bind much less effectively.

The average length of the stopping period is independent of the size of a repellent stimulus and furthermore independent of whether the repellent stimulus was received via SRI or SRII (14). Therefore, in the Petri Net (Model 2), only transitions T_{RS1} and T_{RS2} are controlled by sensory input, whereas the other transitions are not under sensory control and instead are determined by intrinsic properties of the flagellar motor assembly. Thereby each Run phase must itself consist of several states because the spontaneous probability distribution of run-lengths shows a more complicated characteristic than an exponential distribution of a first-order reaction (27).

Refractory and Competent phases

Refractoriness is ubiquitous in sensory physiology. It describes the phenomenon that, after having responded to a stimulus, an organism, for a certain period of time, is either not responsive, or else not fully responsive, to a stimulus of a strength sufficient to have caused the response before. In principle, refractoriness can be caused by the receptor, the signal transduction system, or the effector system. In *Halobacterium*, refractoriness was shown to be an intrinsic property of the flagellar motor switch (28). Directly after the flagellar motor assembly has spontaneously switched its rotational sense, a repellent stimulus that normally would cause motor switching within 1–2 s causes no response, or else a strongly delayed one. Thus the Refractory phase (P_{Ref1} and P_{Ref2}) is inserted directly downstream of the corresponding Stop phase in Model *3* (Fig. 2). In unstimulated cells it lasts for ~1.5 s (28). Subsequently, the Competent phase begins, in which the cell is competent to respond promptly to a repellent stimulus. In a series of elegant experiments, Krohs (29) demonstrated that the transition from the Refractory to the Competent phase is a stochastic process.

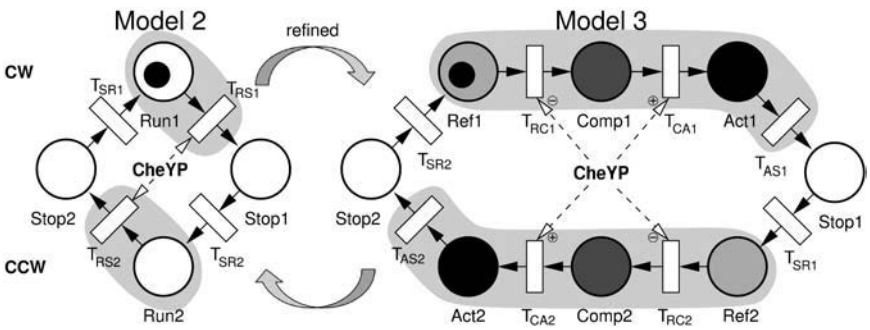

FIGURE 2 Petri Net models of flagellar motor switching. Model *3*: Petri Net model of all eight functional states of the switch complex as derived in this work. Model *3* results from refining the Run places and the adjacent downstream transitions of Model *2* to Refractory, Competent, and Active phases for the CW and the CCW rotational senses. The probability that transitions the T_{CA1} and T_{CA2} switches is positively regulated by the concentration of CheYP, whereas it is negatively regulated for T_{RC1} and T_{RC2}. This influence is symbolized by the arrows and a plus or minus sign, respectively.

Active phase

In addition to the Refractory, Competent, and Stop phases a fourth phase of the switch complex can be postulated, based on the results of pulse experiments. Cells were stimulated by single or double blue light pulses of intensity I. On average, the response time t_R, counting from the onset of the stimulus until the stopping of the cells, is given by

$$t_R = t_{min} + \frac{b}{I(\tau_1 + \tau_2)} + \frac{\tau_2}{(\tau_1 + \tau_2)} \cdot D; \quad \tau_1 + D + \tau_2 > t_R - t_{min}, \tag{1}$$

where τ_1 and τ_2 are the durations of the first and the second pulse, respectively; D is the duration of the dark interval between the two pulses; and b is a constant (27). This result revealed the existence of a rate-limiting, stimulus-independent ''dark process'' that is responsible for a minimal time t_{min} ($\sim$1 s) that is, on average, needed to respond to a repellent signal no matter how strong it might be (27). Equation 1 suggests that the effect of the stimulus which is proportional to $I\tau_1$ and $I\tau_2$ is integrated at the switch complex starting from the time-point of delivery until the threshold b is reached. Thereby the durations τ_1 and τ_2 of both pulses are considered to be short as compared to the response time t_R. Finally, the motor stops rotation at constant time t_{min} after the threshold b is crossed. Equation 1 does not represent spontaneous motor switching, but it can easily be extended by this feature by introducing a constant slope c of the signal integration process:

$$t'_R = t_{min} + \frac{b}{c + I(\tau_1 + \tau_2)} + \frac{\tau_2}{c/I + (\tau_1 + \tau_2)} \cdot D; \quad \tau_1 + D + \tau_2 > t_R - t_{min}. \tag{2}$$

Due to the fact that a spontaneous reversal, on average, occurs only after $\sim$12 s (depending on the experimental conditions) and that the response time for this kind of stimulation is much shorter ($<$2.5 s), the influence of the constant c is neglected in the following.

The process responsible for t_{min} could either be part of the reactions leading to signal formation, e.g., saturating effects, or could directly be a part of the switching process. The following fact favors the switching process as the responsible element: The mean reversal time t_R is linearly dependent on the reciprocal total light exposure ($I(\tau_1 + \tau_2)$), and, additionally, the second pulse is exactly as effective as the first pulse (allowing for its delayed application). This linear dependency contradicts nonlinear saturating effects inside the signal transduction chain that could account for t_{min}. If the first pulse would already saturate the signal formation to some extent, the following second pulse would only have a reduced effectiveness and would lead to a nonlinear influence of the dark interval D. Any hypothetical saturating mechanism due to its nonlinear characteristics contradicts Eqs. 1 and 2 and has been ruled out by simulation (see Ref. 30, Model *a*). Additionally, the following consideration may disfavor a saturating mechanism: Signal formation seems to be similar in eubacteria and in archaea (31); experiments in *E. coli* have shown that signal formation including diffusion from the receptors to the switch complex must be in the range of 10–30 ms (32), and thus, is much too fast for a factor of 30–100. Thus, we propose that a stimulus-independent active switch process is responsible for t_{min} that activates the actual reversing process (analogous to the Models *b* and *c* in Ref. 30). This process is triggered by the preceding stimulus-dependent Competent phase (Fig. 2).

In the framework of the Petri Net formalism the newly derived phases are represented by resolving transitions T_{RS1} and T_{RS2} and places P_{Run1} and P_{Run2} of Model *2*: For each rotational sense, two stimulus-dependent transitions are introduced, joining places representing the Refractory, Competent, and the Active phases (Fig. 2). The refined Petri Net Model *3* (Fig. 2) can be understood as follows: immediately after switching of motor rotation from Stop to CW, the motor is in the Refractory CW (P_{Ref1}) phase (indicated by the token in this place). In unstimulated cells, the refractory period would take $\sim$1–2 s and is prolonged by a repellent stimulus. A repellent stimulus, however, exerts the opposite effect on the subsequent Competent CW (P_{Comp1}) phase. Here a repellent stimulus accelerates the transition to the Active phase before the motor stops during P_{Stop1}.

Symmetry

Model *3* at this point does not describe the characteristics of the transitions. However, its structure is completely symmetric, inasmuch as the transitions indexed with *1* or *2* behave kinetically identically. The symmetry of Model *3* is based on the following experimental results on spontaneous and stimulus-modulated motor switching:

1. Without being stimulated, the cells on average spend equal times in the CW and in the CCW rotational sense (13,33).
2. The run-length of a given interval does not depend on the run-length of the preceding one (28,33).
3. The time-course of the probability for spontaneous switching during a swimming interval is the same for CW and for CCW rotations (14), i.e., the frequency distributions of the run-lengths of unstimulated cells are identically in the two rotational modes (34).
4. Sensory stimuli are equally effective in increasing or decreasing the probability for motor switching in each rotational sense (33).

Hence, the switch complex behaves symmetrically in the absence of stimuli as well as in response to stimulation.

Identification of the number of rate-limiting reactions

The Petri Net of Model *3* does not make predictions of how the transitions switch in a time-dependent manner. By

replacing all transitions by first-order rate constants, it is not possible to reproduce the frequency distribution of spontaneous motor switching, regardless of which set of rate constants is used.

However, the frequency distribution can be reproduced by assuming that the switch complex is composed of multiple subunits and by further refining each functional state of the switch cycle into multiple reaction steps. Instead of further refining the Petri Net model and specifying the transitions, we will now move to the kinetic representation of a mechanistic model, where the probability for the transition between the states depends on the number of CheYP molecules bound to the switch complex. The question then arises of how many rate-limiting reaction steps are necessary to enter each phase of the switch cycle.

The frequency distribution of the duration of each phase could help to answer this question. Unfortunately, only the Stop phase is directly observable. Fig. 3 shows the frequency distribution of Stop durations in half-logarithmic scale. The approximately linear decrease suggests that during the Stop phase the cells resume swimming in the reverse rotational sense with a constant probability per unit of time. Therefore, transitions T_{SR1} and T_{SR2} in Model *3* can be described best by a first-order rate constant. Although the frequency distribution of the duration of the Competent phase is not directly accessible, it can be approximated to the frequency distribution of the total run-lengths for spontaneous reversals, because in unstimulated cells the duration of the Competent phase is much longer (≈10 s) than the duration of the Refractory (≈1.5 s) or the Active phases (≈1 s).

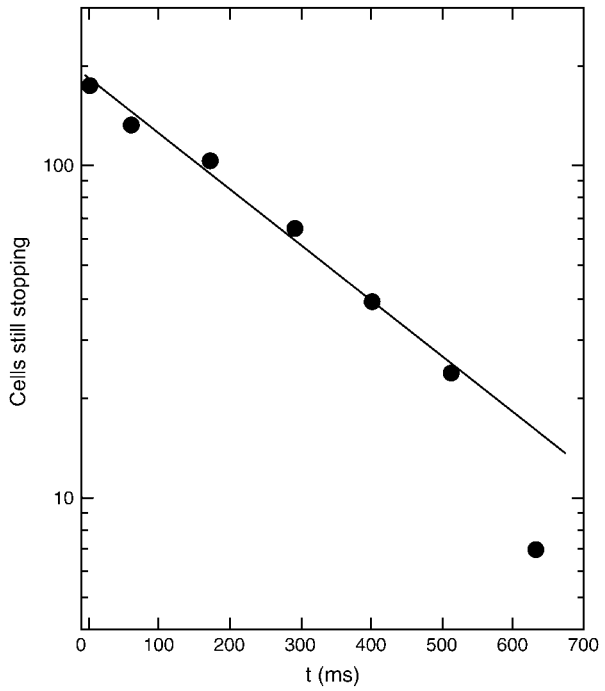

FIGURE 3 Distribution of Stop times in a cell population. The length of intervals cells spent in the Stop state were measured as described for Fig. 1 *B* and the number of cells still stopping at time *t* plotted against time. The dashed line shows the best fit of the data to an exponential distribution, suggesting that the termination of the Stop phase occurs with a constant probability per unit of time. Experimental data were taken from Marwan et al. (14).

The frequency distribution of run-lengths of unstimulated cells exhibits an asymmetric characteristic. Immediately after resuming rotation, the probability for the next spontaneous stopping event remains close to zero for a few seconds, then rises to quickly approach its maximum, then remains constant—resulting in an exponential decay in the frequency distribution of run-length intervals (14,27,28,33).

To estimate the number of rate-limiting steps necessary to describe this behavior, we first use a simplified model (Model *4*; see Fig. 4) that lacks the Refractory phase and models the Competent phase with a number of (n_a) association steps. Furthermore, we make the simplified assumption that, immediately after motor switching, the switch complex is in Competent phase and all (n_a) binding sites are empty and free to bind CheYP. The binding reactions are considered as irreversible and occur in parallel with an equal rate constant, i.e., without a cooperative effect. A further simplifying assumption, which will be relaxed in the final detailed kinetic model, states that the Active phase starts only after all binding sites are occupied by CheYP. In the case of spontaneous reversals, the Active phase is much shorter than the Competent phase. Therefore, its contribution to the frequency distribution is low and can be described by a single first-order reaction with a mean duration of 0.95 s. After the Stop phase, the next swimming interval begins in reverse rotational sense, and it is assumed that CheYP hydrolyzes and CheY dissociates from all binding-sites simultaneously.

This model represents a Markov chain in which each state is interpreted as the probability that the switch complex is in the corresponding state. A single deterministic simulation starting from a given initial probability of each state provides the frequency distribution of the process duration, whereas thousands of stochastic simulations would be required to obtain the same result. This distribution is equivalent to the first-passage-time of the process (35), and is determined by the transition rate of its final step—what is, in this case, the transition rate from Active to Stop.

Fitting the measured frequency distribution of spontaneous run-lengths to the model resulted in a best fit for $n_a = 10$ irreversible binding steps (Fig. 5 *A*). This means that ~10 rate-limiting reactions are necessary to account for the lifetime of the Competent phase.

The number of steps necessary to proceed through the Active phase will be estimated by fitting Model *4* to a frequency distribution of run-lengths in response to a repellent stimulus (Fig. 5 *B*; see also Ref. 33). In this experiment, cells were stimulated with a step-up of UV-light which was applied at 2 s after a spontaneous motor reversal. At this time, the cells have passed through the Refractory phase and are now in the Competent phase, for which we keep the optimized parameters n_a and k_a constant. Due to the

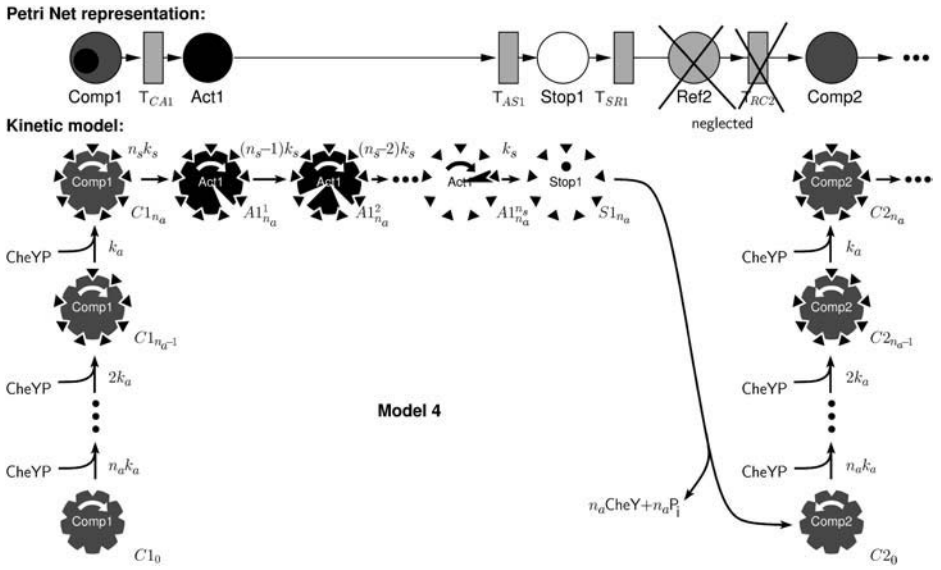

FIGURE 4 Kinetic model used to estimate the number of rate-limiting reaction steps during the Competent and the Active phases (Model *4*). Note that the Refractory phase is neglected in this model and that binding and dissociation of CheYP occurs irreversibly at all subunits.

light-induced increase in intracellular switching signal (CheYP) concentration, the Competent phase becomes much shorter than for adapted conditions. Therefore, the Active phase strongly determines the frequency distribution of motor reversals, and is accordingly modeled in more detail by n_s parallel elementary steps, which have to occur before the Stop phase is entered. The reaction rate k_s is adjusted so that the mean total duration of the Active phase of 0.95 s remains constant. The best fit to the experimental data is obtained for $n_s = 44$ elementary steps. According to the simulation, ~10 binding events have to occur to make all (~44) subunits of the motor stop and then switch the rotational sense.

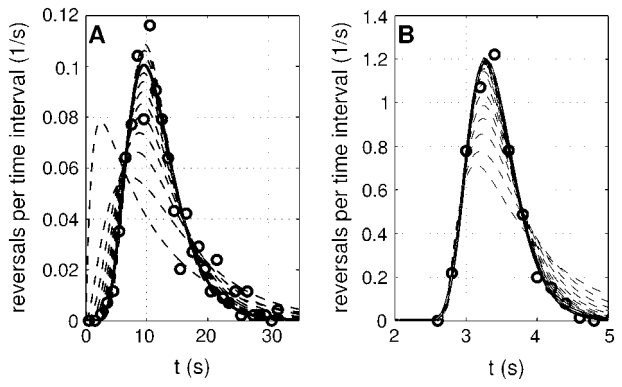

FIGURE 5 Frequency distributions of spontaneous (*A*) and UV-light-induced (*B*) run-lengths and their simulation using Model *4*. The open circles show the experimental results taken from Schimz and Hildebrand (33). (*A*) Spontaneous case. Simulation results of Model *4* with parameter k_a fitted to the experimental data for varying numbers of binding sites ($n_a = 1\ldots13$; *dashed lines*). The best fit was obtained for $n_a = 10$ binding steps and $k_a = 0.27\,s^{-1} \cdot [CheYP_{ss}]$ (*solid line*). (*B*) Repellent stimulation with a step-up in near-UV-light intensity at $t = 2$ s after a spontaneous reversal. Simulation results of Model *4* are shown, with optimal values of n_a and k_a from *A* and optimized parameters for varying number of elementary steps n_s that have to be completed in the course of the Active phase, until the switch complex can enter the Stop phase ($n_s = 1\ldots50$; *dashed lines*). The elementary steps occur with constant probability per unit of time in parallel, and independent of each other (without cooperativity). The lifetime of the Active phase was kept constant, irrespective of value of n_s tested in a given simulation by setting the rate constant for an elementary step to occur to $k_s = 1.054\,s^{-1}\left(\sum_{i=1}^{n_s} i\right)^{-1}$. In the simulation, for technical reasons, the elementary steps were allowed to occur sequentially rather than in parallel.

Model *4* is able to reproduce the response to single- and double-pulse blue-light stimuli in the way predicted by the empirical Eq. 1 (27) (not shown). However, Model *4* cannot reproduce the cellular response to sensory stimuli during the refractory phase of the flagellar motor, because this functional phase was deliberately neglected for a first estimate.

A refined kinetic model for motor switching: Model *5*

On the basis of Model *4*, we now develop a refined kinetic model of motor switching including the Refractory phase and additionally make more realistic assumptions than made for Model *4*. We assume that the switch complex consists of 44 subunits ($n_s = 44$) that each can bind CheYP in a parallel manner. In contrast to Model *4*, binding is now considered to be reversible. The probabilities for dissociation, which may include a hydrolysis step in the Refractory phase, and association of CheYP with each subunit in the Competent phase, are independent of the number of bound CheYP molecules; that is, there is no binding cooperativity. A cooperative mechanism, however, ensures that all subunits are synchronously in one of the functional phases only: Refractory, Competent, Active, or Stop. The occupancy level of bound CheYP influences the probability to switch from Refractory to Competent and from Competent to Active.

In the following, the most probable propagation of Model *5*, as shown in Fig. 6, is discussed. Directly after switching the rotational sense, the switch complex is in the Refractory

phase and highly occupied with CheYP, resulting in a low probability of transition to the Competent phase. Instead, net dissociation of CheY is expected for stationary intracellular CheYP concentrations because the stability of bound CheYP is assumed to be low during Refractory phase. The lower the occupancy with CheYP, the higher the probability for a cooperative conformational change of the switch complex to the Competent phase, which occurs stochastically with the first-order rate constant k_1. The negative exponential dependency of k_1 on the number of CheYP molecules bound to the switch complex (Y_{bound}) is given by

$$k_1 = k_1^0 \cdot e^{-iR}; i = Y_{\text{bound}}, \quad (3)$$

where k_1^0 and R are constants. Equation 3 assumes that, although the overall conformational change in the switch complex synchronously comprises all subunits, those which have CheYP bound cooperatively inhibit the change to the Competent phase. On average, the transition to the Competent phase occurs within 2 s after switching the rotational sense.

In the Competent phase, the affinity of the subunits of the switch complex to CheYP is higher than during the Refractory phase, now leading to net binding of CheYP even at constant CheYP concentration (in adapted or unstimulated cells). With increasing occupancy level, the probability for a stochastic transition from the Competent to the Active phase increases as well. The transition probability is given by

$$k_2 = k_2^0 \cdot e^{iC}; i = Y_{\text{bound}}, \quad (4)$$

where k_2^0 and C are constants. The exponential term in Eqs. 3 and 4 accounts for the cooperative mechanism that facilitates the conformational change from Competent to Active. In contrast to Model *4*, the transition can occur with any number of bound CheYP molecules. On average it takes ~9 s, according to the simulation results.

During the Active phase, each subunit undergoes a conformational change with a first-order rate constant in a parallel, irreversible, and noncooperative manner. The Active phase including all conformational changes takes ~1 s. After all conformational changes have occurred, the switch complex cooperatively enters the Stop state, from which it proceeds with a first-order reaction to the Refractory phase of the opposite rotational sense. For simplicity, CheYP association or dissociation is not considered during the Active and Stop phases.

Simulation of the spontaneous behavior and of light-regulated motor switching using Model *5*

We will now show that the results of different types of behavioral experiments published over the past 20 years can be quantitatively reproduced by Model *5*. Since part of these experiments was performed by stimulation of the cells with orange or UV-light that is perceived via sensory rhodopsin I (SRI), and in some experiments light stimulation lasted so long that excitation and adaptation overlap, the kinetic model for the excitation pathway as controlled by SRII (30) was expanded. Depending on the stimulus type, a model of the SRI·HtrI complex or the SRII·HtrII complex was used, and an adaptation feedback loop by the CheA kinase-regulated methylesterase CheB and the nonregu-

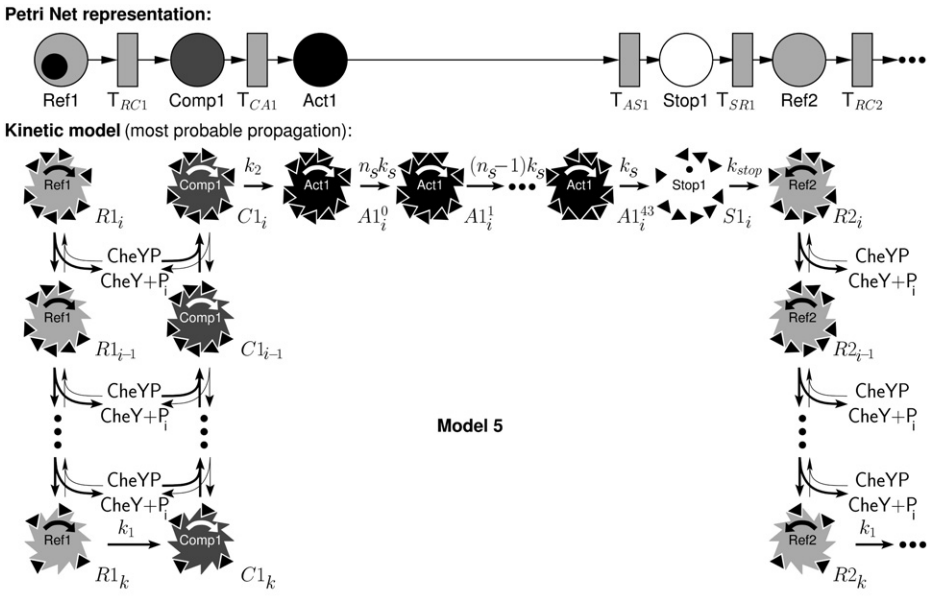

FIGURE 6 Model *5*: Most probable propagation of the detailed Kinetic model of the switch complex comprising all functional states from Model *3*. The switch complex occurs in four different conformational states for each rotational sense as indicated by the Petri Net representation above. Solid triangles represent binding-sites of the switch complex bound with CheYP. Their orientations represent the conformational state of the complex. Different shades of the complex indicate their functional state. An arrow or dot inside the complex shows the rotational direction of the motor. During the Refractory phase, CheYP most likely dissociates from the complex under hydrolysis, increasing the probability for a transition to Competent phase. Here bound CheYP is more stable, leading to net association and increasing probability to proceed to Active phase. During the Active phase all n_s subunits change their conformational state before the motor proceeds through the Stop state to the Refractory phase of the reverse rotational sense. For simplicity, binding or dissociation of CheYP is not modeled during the Active and Stop phases. For clarity, only one possible propagation through Model *5* is shown.

lated methyltransferase CheR was introduced (Model *6*; for details see legend to Fig. 7). Note that Model *6* is very preliminary in terms of the adaptational mechanism. It can only exhibit adaptation in the sense of resetting an excitation signal, as required for this work. Although the true adaptation system in *Halobacterium* involves CheR and CheB (as assumed in the model), the feedback mechanism is presumably more sophisticated and very likely involves additional proteins like CheD or the CheJs (see Ref. 2; see also http://www.halolex.mpg.de).

The frequency distributions of run-length intervals

The frequency distributions of the run-lengths of non-stimulated cells and of cells stimulated with a step-up in UV-light (repellent stimulus) or a step-down in UV-light (attractant stimulus) in white observation light were measured (33). At the time-point of stimulation, the cells had recovered from the refractory phase and were fully responsive, whereas nearly none of the cells had reversed spontaneously. Fig. 8 *A* compares the experimental data with simulations performed with Model *6* (excitation and adaptation) coupled to Model *5* of the flagellar motor switch complex. Fig. 8 *B* shows the time-course of the CheYP concentration after UV-light step-up and step-down stimulation as obtained through parameter optimization.

Fig. 9 shows the frequency distribution of interval lengths between spontaneous motor switching events correlated with the time-courses of the mean reversal probability and of the mean occupancy level of the switch complex subunits with CheYP. Beyond the maximum of the frequency distribution (Fig. 9 *A*), both the mean occupancy level and the reversal probability have almost reached their final constant level. This indicates that at that time, the switch complexes of nearly all cells that have not yet switched the rotational sense, have a constant mean number of CheYP molecules bound, and thus proceed to the Active phase with constant probability per unit of time, subsequently entering the Stop phase. The first-order reaction for entering the Active phase dominates this process and is visible as exponential decay of the frequency distribution. The activation energy for spontaneous motor switching of 73 kJ/mol as determined by measuring the temperature dependence of this exponential decay (27) can now be assigned to the conformational change from the Competent to the Active phase of Models *4* and *5* under unstimulated conditions. It determines the overall rate-limiting step of the motor switch, mainly responsible for t_{min} (Eq. 1).

The response to single- and double-pulse stimulation

When dark-adapted cells are exposed to a short pulse of blue light that is received by SRII, the response depends on the photon exposure of the pulse (the number of photons applied to the cells, which is proportional to the light intensity × the pulse duration). If the photon exposure is very low, the cellular response is stochastic and the stimulus-response-curve

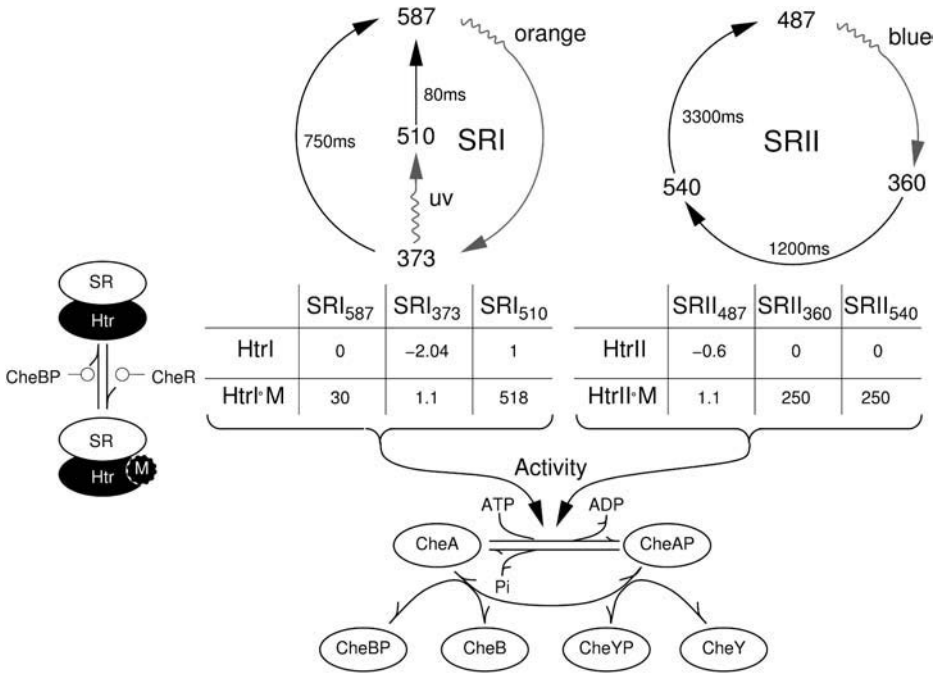

FIGURE 7 Simple kinetic model of the phototaxis signaling network based on a two-component system. The model consists of four modules: receptor, methylation state, activity calculation, and phosphorylation chain. It works for SRI·HtrI or SRII·HtrII only, i.e., does not account for integration of stimuli applied through the two photoreceptors. Receptors: The wavy arrows represent photoreactions. The half-life of each photointermediate state is given with the plain arrows. Methylation: Methylation is mediated by CheR at a constant rate. CheBP demethylates the transducers at a rate proportional to the CheBP concentration (i.e., CheBP works at V_{max}). Activity: The fraction of receptors in a certain state and the fraction of methylated or demethylated transducers determine the activity of the receptor complexes according to the given table. Phosphorylation chain: Phosphorylation reactions are assumed to be fast. Therefore their dynamics have been neglected and instead a linear correlation for the activity and the concentration of CheYP or CheBP is used, respectively, up to a minimal and a maximal value. In light-adapted cells the activity equals 1. For higher activities, demethylation is stronger than methylation, leading to a lower methylation level and, in turn, to a lower receptor activity.

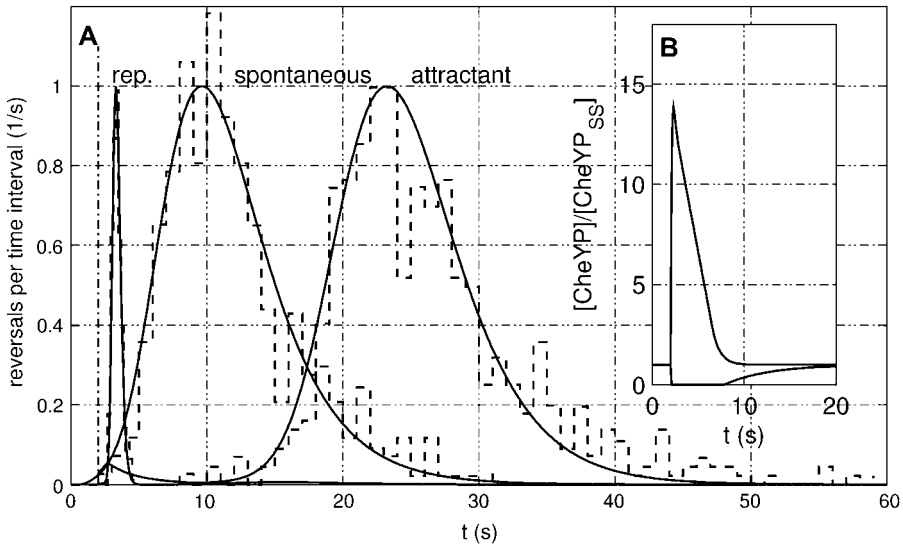

FIGURE 8 (*A*) Measured (*dashed lines*) and simulated (*solid lines*) frequency distributions of swimming interval lengths for spontaneous reversals and repellent or attractant stimulation, as indicated. The stimulus was applied at $t = 2$ s (*dashed-dotted line*). Each frequency distribution is normalized with respect to the maximum. To simulate the behavioral response to light, the kinetic model of the switch complex (Model *6*) was coupled to the kinetic model of the phototaxis signaling network (Model *7*) via CheYP. (*B*) Simulated time-course of CheYP for repellent (*positive* peak) and attractant (*negative peak*) stimulation. Experimental data taken from Schimz and Hildebrand (33).

follows a Poisson distribution (36). Slightly higher light intensities, just high enough to make all cells respond to the stimulus pulse, are not saturating signal transduction. If the intensity of the stimulus pulse is further increased, the cells respond more quickly to the stimulus, as discussed before. As predicted by the Eq. 1, straight lines are obtained by plotting the mean response time of the cells against $1/I$, the pulse ratio $\tau_2/(\tau_1 + \tau_2)$ or the dark interval D, respectively (Fig. 10, *A–C*). The kinetic model of the switch complex (Model *5*) is able to reproduce the response to double-pulse stimulation. As concluded from the optimized parameter set, t_{min} ($\approx$0.95 s) mainly results from the transition from the Active to the Stop state (which takes 0.62 s) rather than from upstream processes like CheYP generation or binding of CheYP to the subunits of the switch complex in the Competent phase.

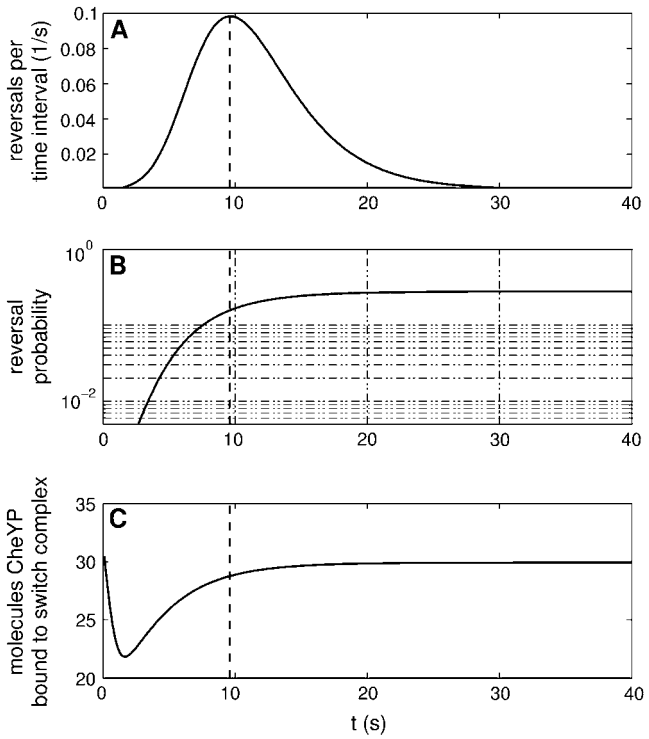

FIGURE 9 Spontaneous motor switching. Correlation of the frequency distribution of run-length intervals (*A*), with the mean reversal probability (*B*) and the mean number of subunits of the switch complex that have bound CheYP (*C*), as calculated using Model *6*. Dashed lines indicate the time-point of maximal reversal probability.

The response to repellent stimulation during and after the refractory period

In a series of experiments, Krohs (29) studied the response of cells to repellent stimulation during the Refractory period after spontaneous motor switching (28,33). A steplike repellent stimulus was applied with random delay time (t_d, as chosen by a computer) after a spontaneous reversal, and the time interval t_r until the next motor reversal was measured. The repellent stimulus was either a step-down in orange light or a step-up in near UV (in the presence of orange background light) or blue light, and each of these stimuli qualitatively produced the same experimental results. When the individual response times of the cells (i.e., the time interval elapsed between stimulus application and motor response) were plotted against the delay time between the last spontaneous reversal and stimulus application, it became obvious that the values fell into two well-separated groups (Fig. 11). When stimulated after the refractory phase (2 s after the spontaneous reversal or later), the cells responded within $\sim$2 s to the stimulus. However, cells stimulated within the refractory phase frequently did respond to the stimulus much later. Analysis of this late-responding population of events (it is a stochastic decision of a single cell and not due to variations within a population of cells) revealed that the

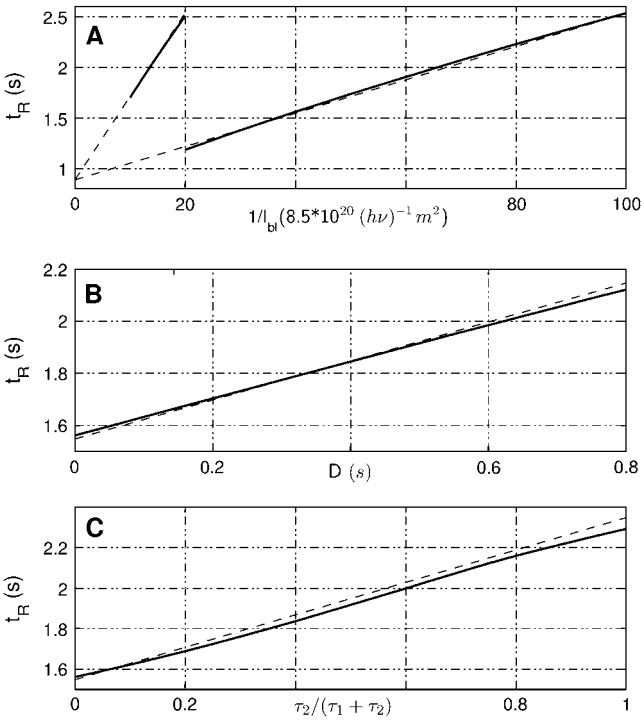

FIGURE 10 Simulated mean response-time (*solid lines*) and mean response-time as predicted by Eq. 1 (*dashed lines*) to single- and double-pulse repellent-stimulation with blue light perceived by SRII. Note that optimal simulation results were obtained by setting the half-lives for SRII states to values 10-fold longer than the values measured in membrane vesicles (Ref. 50, and references therein). (*A*) Mean response time t_R of cells to a single pulse of $\tau = 20$ ms or $\tau = 100$ ms of photon irradiance I, plotted against $1/I$. (*B*) Mean response time t_R of cells to two pulses of equal intensity but different pulse duration. The two pulses were delivered before the response of the cell had occurred. The duration of the first pulse was $\tau_1 = 25$ ms, that of the second pulse was $\tau_2 = 75$ ms, and the dark interval D between the two pulses was varied. As predicted by Eq. 1, the slope of the curve is $\tau_2/(\tau_1 + \tau_2) = 0.75$. (*C*) Mean response time t_R of cells to two pulses of equal intensity but different ratio in $\tau_2/(\tau_1 + \tau_2)$. As predicted by Eq. 1, the slope of the curve corresponds to the dark interval between the two pulses of $D = 800$ ms. Simulations were performed with Model *6* coupled to Model *7*.

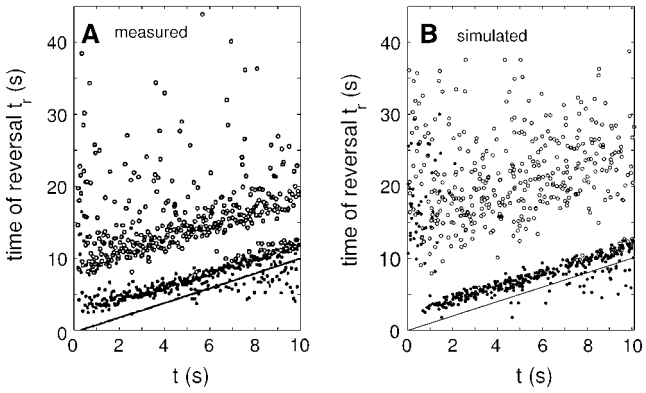

FIGURE 11 Variation of the delay t_D of a repellent orange light step-down after the preceding spontaneous reversal at $t = 0$ s. The time-points of the first reversal (*dots*) and the second reversal (*circles*) are plotted against the delay t_D of the stimulus. Solid lines indicate the stimulus onset. (*A*) Measurements taken from Krohs (29, Fig. 4 *A*). (*B*) Simulation results. The discrete time-points of reversals were taken randomly from the probability distributions obtained by simulation of Models *6* and *7*.

frequency distribution of run-lengths of the stimulated cells in the Refractory phase drastically deviated from the frequency distribution of nonstimulated cells, indicating that the cells during the Refractory phase indeed responded to the stimulus applied, but with a delay (29). By observing not only the first reversal, but several successive reversals, it was shown that a steplike repellent stimulus results in a damped oscillation of the time-points of switching, occurring with a period length of ~5 s. The oscillation is detectable for up to 15–20 s. By triggering the damped oscillation through stimulus application at various time intervals after a spontaneous reversal, Krohs (29) showed that the oscillation occurred irrespective of the state in which the switch complex found itself, and that the second reversal after a prompt, non-refractory one was equivalent in its distribution to a refractory reversal. The results in addition suggested that there is no feedback between the switch complex and the signal transduction network, and that damped oscillations in the switching signal (presumably CheYP) have to be assumed to explain these observations.

In contradiction to this conclusion, our kinetic model of the switch can reproduce his experimental results at first approximation for the first and for the second reversal in response to a stimulus (*dots* and *circles* in Fig. 11), without assuming damped oscillations in the switching signal. In our simulations CheYP simply declined to the stationary level through adaptation (see Fig. 8 *B*). The observed damped oscillations in the reversals (best seen for *dots* and *circles* at $t_D = 0$–1 s in Fig. 11) arise due to the effect that the switch complex in each cell is in the same state at the beginning of the experiment ($t_D = 0$ s), but then asynchronously proceeds through the subsequent states. Furthermore, the observation of equal probability distributions of refractory reversals and next-to prompt reversals (compare *dots* at $t_D = 0$ s with *circles* at $t_D > 2$ s in Fig. 11) is described by our model as well. It results from the refractory phase in which a high CheYP concentration inhibits the transition to the Competent phase, thereby delaying the next switching event (compare with Model *3*, Fig. 2). This mechanism equally occurs in cells that are in the Refractory phase during stimulation and in cells that are forced to proceed to the Refractory phase (via a reversal) by the stimulus.

The experimental results of Krohs (29) put an important kinetic constraint on our kinetic model of the switch. The gap in the frequency distribution during the refractory phase (Fig. 11, *dots*), as obtained in the experiments in response to any of the three stimulus types (orange step-down, UV step-up, and blue step-up) could only be reproduced by model simulation, if the changes between the Refractory, Competent, and Active phases were modeled as irreversible transitions that occurred synchronously in all subunits of the

switch complex. In other words, according to the simulation, it is not possible that some of the subunits are already in the Active phase while others are still binding CheYP or some are binding CheYP, being in the Competent phase, and others are still Refractory. Therefore, this important feature of the model, synchrony of the subunits with respect to conformational changes, which might be regarded as an arbitrary assumption, results from experimental and computational evidence.

Inverse response to attractant pulse stimulation

When dark-adapted cells are exposed to an attractant orange-light pulse, they respond by reversal suppression as expected. However, if the orange light pulse is delivered to cells that had responded to a step-down in orange light some seconds before, the second stimulus now acts as a repellent and causes motor switching instead of reversal suppression (28). This effect was observed when the orange-light pulse was delivered up to 6 s after orange-light step-down (Fig. 12). In a strain that contained both SRI and SRII, a step-down in orange light inverts the reversal-suppressing effect of a step-down in blue light to reversal-inducing, indicating that post-receptor processes which are independent of a specific receptor system are involved in generating the inverse response (28). The same effect is observed when this experiment is performed in silico with our kinetic model of the switch. The repellent orange off-signal at $t = 0$ s causes a high CheYP concentration, which in turn causes most cells to reverse. Subsequently, the switch complex of the cells that reversed is trapped in the Refractory phase, because the high CheYP concentration inhibits the transition to the Competent phase. If an attractant pulse is applied during this time, the CheYP-level transiently drops, causing net dissociation of CheYP from the switch complex and facilitating the transition to the Competent phase (see Fig. 6). After the attractant pulse, the CheYP concentration rises well above the CheYP level of adapted cells. This rise of CheYP is still caused by the first stimulus (orange step-down). Because methyltransferase and methylesterase work so slowly, the transducers that have been methylated during adaptation to constant orange light now in the dark are overmethylated, as compared to the adapted state, enhancing the rate of CheY phosphorylation even several seconds after the step-down.

DISCUSSION

Several models of the halobacterial flagellar motor switch have been published, each of them accounting for different experimental aspects. The model formulated by McCain et al. (28) contained three functional states—Inactive, Nonreversing, and Reversing. The Inactive and the Nonreversing states in the McCain model correspond to the Refractory and the Competent states of our model, respectively. But because the transition from Inactive to Nonreversing was assumed to be stimulus-independent and because the transitions between the three states are controlled by first-order rate constants, the explanatory power of this model is limited. The model of Marwan and Oesterhelt (27) described the frequency distribution of spontaneous reversals by an autocatalytic process of the switch assembly without considering stimulus-induced reversals or refractory effects. The model by Naber (35), in several respects, behaves similarly to the model developed by Nutsch (30); both models cannot reproduce the effect of the refractory period without making non-straightforward assumptions on the time-course of the switching signal. None of the kinetic models of motor switching in *E. coli* (37,38) could reproduce even a single experimental result on halobacterial flagellar motor switching (not shown). Therefore, a new modeling approach was necessary.

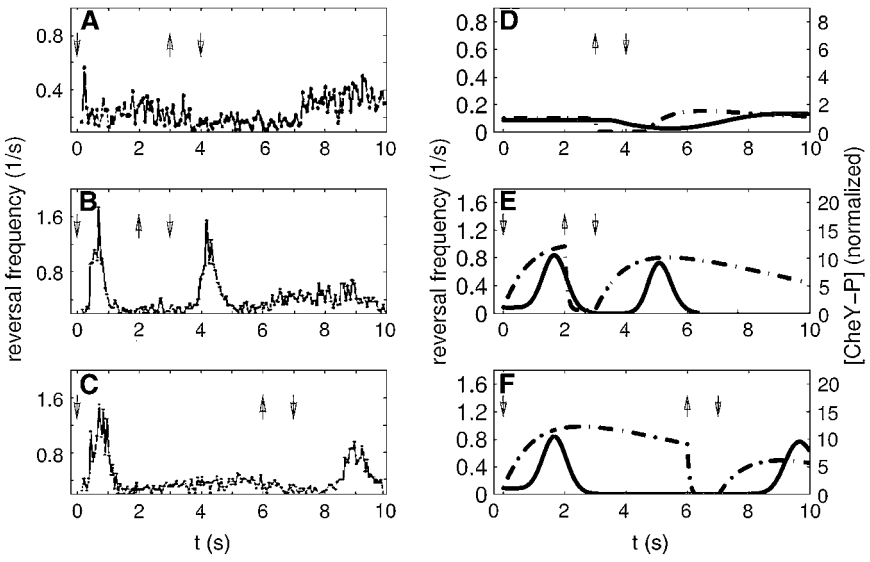

FIGURE 12 Measured (*A–C*) and simulated (*D–E*) response to an orange-light pulse without (*A*, *D*) and with (*B*, *C*, *E*, and *F*) switch-off of orange light at $t = 0$ s. Measurements were taken from McCain et al. (28, Fig. 6). (*A* and *D*) Dark-adapted cells respond to a single orange-light pulse with transient reversal suppression-attractant response. (*B*, *E*, *C*, *F*) When cells pre-adapted to orange light are exposed to a decrease in orange light followed by the same pulse that caused an attractant response in *A* and *B*, the pulse now causes an inverted (i.e., repellent) response. On and off of orange light is indicated by arrows. (*Solid lines*) Simulated reversal frequency. (*D–F*) (*Dash-dotted lines*) Simulated CheYP concentration normalized to the level in unstimulated cells.

Table 3 compares all published models of the flagellar motor switch and its sensory control in *Halobacterium* regarding their ability to quantitatively reproduce the behavioral responses. The table also compares the qualitative structural properties of the different models. Only the model presented in this work is able to quantitatively reproduce all experimental results tested. Interestingly, the model by McCain et al. (28) displays nearly all structural features of our model, although it completely fails in reproducing the experimental results quantitatively. And although the later models by Naber (35) and Nutsch (30) were considerably better in reproducing the behavior of the switch complex quantitatively, important structural properties were still missing. Considering this development, the table suggests that a direct and efficient way of reverse-engineering biochemical reaction networks might be to first generate a model structure (represented, e.g., as a Petri Net), which reproduces experimental results qualitatively and then, step by step, refine this structure by generating a kinetic model, able to quantitatively reproduce the results obtained in the experiments. We did start from the simplest possible description and then, step by step, introduced additional functional states as derived from experimental observations until the general behavior could be finally described by the eight functional states of Model *3*. We then estimated the number of rate-limiting steps for each underlying process necessary to describe its kinetic behavior. The probability distribution of the duration of the Stop phase could thereby best be described by a single first-order reaction. The best representation for the Competent phase as derived from Model *4* was $n_a = 10$ parallel association reactions and $n_s = 44$ independent, parallel reactions for the Active phase.

These results raise the question of which underlying mechanism could possibly incorporate ~10 and 44 reaction steps at the same time. Following the model of conformational-spread applied to motor switching in *E. coli* (38), we came to the conclusion that the switch complex could consist of ~44 subunits that each can bind CheYP, and that its occupancy level might control the transition probability to the subsequent functional states. In contrast to the model of conformational-spread, our model is not in equilibrium—a necessary consequence from the fact that the switching process in halobacteria is cyclic. The most probable explanation is the postulation that the genetic deficiency of *H. salinarum* for CheZ, the soluble, CheYP hydrolyzing enzyme of *E. coli*, is a property of the switch subunits in the refractory conformational state. This would provide the intrinsic energy supply for the halobacterial (archaeal) motor-switch cycle. If the hydrolysis of CheYP indeed should be the energy-providing step, then switching should not occur in CheY molecules where the phosphorylation site has been deleted. But since there are no such mutants available, the experiment cannot be performed at present. By proposing that the probability of the transition from Refractory to Competent and from Competent to Active is exponentially dependent on the number of CheYP molecules bound to the switch complex, and thus these transitions are not only possible when all subunits have bound CheYP, on average ~10 dissociation and association reactions (compare with Fig. 9) during the Refractory and the Competent phase are sufficient to cause a conformational change of all 44 subunits during the Active phase.

The detailed kinetic model presented here (Model *5*), in combination with a simple adaptational mechanism (Model

TABLE 3 Comparison of the different kinetic models for the flagellar motor switch of *H. salinarum* and its sensory control

	This work	Nutsch et al. (30)	Naber (35)	McCain et al. (28)	Marwan and Oesterhelt (27)
Quantitative reproduction of behavioral responses*					
Frequency distribution of run-length intervals (spontaneous)	+	+	+	(*a*)	+
Frequency distribution of run-length intervals (attractant, repellent)	+	+	(*b*)	—	—
Response to single and double pulse stimulation	+	+	—	—	—
Delayed response to repellent step-up during refractory phase	+	—	(*c*)	—	—
Inverse response to attractant pulse during refractory phase	+	—	—	—	—
Stopping upon switching motor rotation	+	—	—	—	—
Structural properties of the model†					
Symmetry (CW→CCW; CCW→CW) for motor reversals	+	+	+	+	+
Irreversible cyclic process	+	+	+	+	+
Refractory phase	+	—	—	+	—
Responsive phrase	+	+	+	+	+
Reversing phase	+	+	—	+	—
Stopping phase	+	—	—	—	—
Number of possible states per rotational sense	174	8	16	3	2

*Models evaluated regarding their ability to quantitatively reproduce spontaneous behavior or the response to stimulation (+, yes; −, no). (*a*) The model by McCain et al. reproduces the exponential decay part of the frequency distribution of spontaneous run-length intervals only, not its rise. The model by Naber required special assumption for the time-course of the switching signal to reproduce the frequency distribution after attractant or repellent stimulation (*b*), and to explain the delayed response to repellent stimulation during the refractory phase (*c*).

†Models evaluated regarding their structural features introduced to qualitatively explain the spontaneous motor-switching behavior and the response to stimulation. Note that the switch complex does not assume all 174 possible states during a rotational interval.

6), correctly reproduces all the experimental results on halobacterial motor switching and its sensory control tested so far. It might require changes in certain mechanistic details as new experimental results are available, but these changes presumably will not affect the structure of the Petri Net model (Model *3*).

Some important points essential to the operation of the switch complex, like the nature of the switching signal and the mode of energy input that drives the cycle, were not addressed by our modeling approach. However, note that in *B. subtilis* it has been shown that CheYP is hydrolyzed at the flagellar switch (31).

A yet-unanswered question concerns the nature of the switching signal. Even before the halobacterial transducers were identified to be orthologous to the bacterial methyl-accepting chemotaxis proteins (39,40), it was shown that the photoreceptors are coupled to the flagellar motor assembly through chemical signaling (41)—rather than by a transient change in membrane potential. In search of the chemical signal, a switch factor was isolated, defined by its activity to be able to reconstitute motor switching in a straight swimming mutant, and it was identified chemically as fumarate (42). Subsequently, this switch factor was shown to be released from wild-type cells upon repellent light stimulation (43) and fumarate, as detected by an enzymatic assay, was shown to be released in blue-light-stimulated wild-type cells (300 molecules of fumarate per activated SRII molecule), but not in cells lacking functional sensory rhodopsins (44). Meanwhile it was demonstrated that fumarate acts as switch factor in *E. coli* where it facilitates motor switching by reducing the energy difference between the CCW and the CW conformational phases of the switch (45–47). However, since bacterial and archaeal flagellar motors are built from different proteins, the mechanism of action of fumarate could well be different in both species. On the other hand, our modeling and simulation has not provided any evidence for two signals to be involved in controlling motor switching. The assumption that CheYP regulates motor switching in *Halobacterium* is based on the finding that a deletion mutant in CheY or CheA swims by exclusively rotating its flagellar motor assembly clockwise (2,48), and that halobacterial CheAP is dephosphorylated by halobacterial CheY in vitro (49). However, no change in the phosphorylation level of CheY in response to photostimulation has been shown. Therefore, the biochemical nature of the switching signal in the context of Model *5* remains to be determined. At present, it cannot be excluded that fumarate as the switching signal regulates k_1 and k_2 whereas CheYP is required for CCW flagellar rotation, especially since the biochemical function of several Che proteins is unclear. However, Model *5* will help to understand the behavior of mutants with altered levels of CheY or of fumarate.

Although the model described in this work can quantitatively reproduce all experimental results tested so far, many questions regarding the molecular network mediating phototaxis in *Halobacterium* are still open. The molecular mechanisms of sensory integration of different input stimuli, sensory adaptation to the stimulus background, and the possible role of cross-talk between transducers of different specificity are of immediate interest. Predictions by the model will help to evaluate alternative molecular mechanisms and to design experiments to discriminate between them.

To this end it seems that the switch complex of the flagellar rotary motor of archaea is not only composed of an entirely different set of proteins than the bacterial counterpart (8,9) but it also seems to function with a fundamentally different mechanism, as indicated by the fact that none of the recently published models of the mechanism of motor switching in *E. coli* (37,38) in our hand reproduced motor switching in *H. salinarum*. This suggests that nonredundant information can be obtained by comparatively exploring the molecular mechanisms of archaeal phototaxis and bacterial chemotaxis and even promises valuable insight into the evolution of biological signaling, as the two networks partially are composed of orthologous proteins.

We thank Dr. Ricardo del Rosario for confirming that the computational methods are described in sufficient detail to implement the models and run the simulations without requiring additional information.

REFERENCES

1. Marwan, W., and D. Oesterhelt. 2000. Archaeal vision and bacterial smelling: sensory control of the swimming behavior by two component signaling and fumarate. *ASM News*. 66:83–89.
2. Rudolph, J., and D. Oesterhelt. 1996. Deletion analysis of the *che* operon in the archaeon *Halobacterium salinarium*. *J. Mol. Biol.* 258:548–554.
3. Rao, C. V., J. R. Kirby, and A. P. Arkin. 2004. Design and diversity in bacterial chemotaxis: a comparative study in *Escherichia coli* and *Bacillus subtilis*. *PLoS Biol.* 2:239–252.
4. Oesterhelt, D. 1998. The structure and mechanism of the family of retinal proteins from halophilic archaea. *Curr. Opin. Struct. Biol.* 8: 489–500.
5. Klare, J. P., V. I. Gordeliy, J. Labahn, G. Büldt, H.-J. Steinhoff, and M. Engelhard. 2004. The archaeal sensory rhodopsin II/transducer complex: a model for transmembrane signal transfer. *FEBS Lett.* 564: 219–224.
6. Gordeliy, V. I., J. Labahn, R. Moukhametzianov, R. Efremov, J. Granzin, R. Schlesinger, G. Büldt, T. Savopol, A. J. Scheidig, J. P. Klare, and others. 2002. Molecular basis of transmembrane signaling by sensory rhodopsin II-transducer complex. *Nature*. 419:484–487.
7. Wegener, A.-A., J. P. Klare, M. Engelhard, and H.-J. Steinhoff. 2001. Structural insights into the early steps of receptor-transducer signal transfer in archaeal phototaxis. *EMBO J.* 20:5312–5319.
8. Bardy, S. L., S. Y. M. Ng, and K. F. Jarrell. 2003. Prokaryotic motility structures. *Microbiology*. 149:295–304.
9. Nikhil, A. T., S. L. Bardy, and K. F. Jarrell. 2001. The archaeal flagellum: a different kind of prokaryotic motility structure. *FEMS Microbiol. Rev.* 25:147–174.
10. Alam, M., and D. Oesterhelt. 1984. Morphology, function and isolation of halobacterial flagella. *J. Mol. Biol.* 176:459–475.

11. Silverman, M., and M. Simon. 1974. Flagellar rotation and the mechanism of bacterial motility. *Nature*. 249:73–74.
12. Alam, M., M. Claviez, D. Oesterhelt, and M. Kessel. 1984. Flagella and motility behaviour of square bacteria. *EMBO J*. 3:2899–2903.
13. Hildebrand, E., and A. Schimz. 1985. Behavioral pattern and its sensory control in *Halobacterium halobium*. *In* Sensing and Response in Microorganisms. M. Eisenbach and M. Balaban, editors. Elsevier, Amsterdam, The Netherlands. 129–142.
14. Marwan, W., M. Alam, and D. Oesterhelt. 1991. Rotation and switching of the flagellar motor assembly in *Halobacterium halobium*. *J. Bacteriol*. 173:1971–1977.
15. Baumgarten, B. 1996. Petri Nets—Basics and Applications. Spectrum Academic Publishing, New Orleans, LA.
16. Petri, C. A. 1962 . Communication with Automata. Thesis. Faculty for Mathematics and Physics, Technische Hochschule Darmstadt, Bonn, Germany.
17. Pinney, J. W., R. D. Westhead, and G. A. McConkey. 2003. Petri net representations in systems biology. *Biochem. Soc. Trans*. 31:1513–1515.
18. Rosenstengel, B., and U. Winand. 1991 . Petri Nets: An Application-Oriented Introduction. Braunschweig, Vieweg, Wiesbaden, Germany.
19. Chen, M., and R. Hofestaedt. 2003. Quantitative Petri net model of gene regulated metabolic networks in the cell. *In Silico Biol*. 3: 347–365.
20. Goss, P. J. E., and J. Peccoud. 1998. Quantitative modeling of stochastic systems in molecular biology by using stochastic Petri nets. *Proc. Natl. Acad. Sci. USA*. 95:6750–6755.
21. Heiner, M., and I. Koch. 2004. Petri Net-Based Model Validation in Systems Biology. Springer-Verlag, Berlin. 216–237.
22. Matsuno, H., Y. Tanaka, H. Aoshima, A. Doi, M. Matsui, and S. Miyano. 2003. Biopathways representation and simulation on hybrid functional Petri Net. *In Silico Biol*. 3:389–404.
23. Reddy, V. N., M. L. Mavrovouniotis, and M. N. Liebmann. 1993. Petri Net Representation in Metabolic Pathways. AAAI Press, Menlo Park, Bethesda, MD. 328–336.
24. Srivastava, R., M. S. Peterson, and W. E. Bentley. 2001. Stochastic kinetic analysis of the *Escherichia coli* stress circuit using σ^{32}-targeted antisense. *Biotechnol. Bioeng*. 75:120–129.
25. Voss, K., M. Heiner, and I. Koch. 2003. Steady-state analysis of metabolic pathways using Petri nets. *In Silico Biol*. 3:367–387.
26. Zevedei-Oancea, I., and S. Schuster. 2003. Topological analysis of metabolic networks based on Petri net theory. *In Silico Biol*. 3:323–345.
27. Marwan, W., and D. Oesterhelt. 1987. Signal formation in the halobacterial photophobic response mediated by a fourth retinal protein (P 480). *J. Mol. Biol*. 195:333–342.
28. McCain, D. A., L. A. Amici, and J. L. Spudich. 1987. Kinetically resolved states of the *Halobacterium halobium* flagellar motor switch and modulation of the switch by sensory rhodopsin I. *J. Bacteriol*. 169:4750–4758.
29. Krohs, U. 1995. Damped oscillations in photosensory transduction of *Halobacterium salinarium* induced by repellent light stimuli. *J. Bacteriol*. 177:3067–3070.
30. Nutsch, T., W. Marwan, D. Oesterhelt, and E.-D. Gilles. 2003. Signal processing and flagellar motor switching during phototaxis of *Halobacterium salinarum*. *Genome Res*. 13:2406–2412.
31. Szurmant, H., M. W. Bunn, V. J. Cannistraro, and G. W. Ordal. 2003. *Bacillus subtilis* hydrolyzes CheY-P at the location of its action, the flagellar switch. *J. Biol. Chem*. 278:48611–48616.
32. Lux, R., V. R. N. Munasinghe, F. Calstellano, J. W. Lengeler, E. T. Corrie, and S. Khan. 1999. Elucidation of a PTS-carbohydrate chemotactic signal pathway in *Escherichia coli* using a time-resolved behavioral assay. *Mol. Biol. Cell*. 10:1133–1146.
33. Schimz, A., and E. Hildebrand. 1985. Response regulation and sensory control in *Halobacterium halobium* based on an oscillator. *Nature*. 317:641–643.
34. Marwan, W., M. Alam, and D. Oesterhelt. 1987. The flagellar movement of halophilic bacteria. *Naturwiss*. 74:585–591.
35. Naber, H. 1997. The response of halobacteria to single light stimuli: a theoretical analysis. *Eur. Biophys. J*. 26:163–173.
36. Marwan, W., P. Hegemann, and D. Oesterhelt. 1988. Single photon detection in an archaebacterium. *J. Mol. Biol*. 199:663–664.
37. Alon, U., L. Camarena, M. G. Surette, B. A. Y. Arcas, Y. Liu, S. Leibler, and J. B. Stock. 1998. Response regulator output in bacterial chemotaxis. *EMBO J*. 17:4238–4248.
38. Duke, T. A. J., N. Le Novère, and D. Bray. 2001. Conformational spread in a ring of proteins: a stochastic approach to allostery. *J. Mol. Biol*. 308:541–553.
39. Ferrando-May, E., M. Krah, W. Marwan, and D. Oesterhelt. 1993. The methyl-accepting transducer protein HtrI is functionally associated with the photoreceptor sensory rhodopsin I in the archaeon *Halobacterium salinarium*. *EMBO J*. 12:2999–3005.
40. Yao, V. J., and J. Spudich. 1992. Primary structure of an archeabacteria transducer, a methyl-accepting protein associated with sensory rhodopsin I. *Proc. Natl. Acad. Sci. USA*. 89:11915–11919.
41. Oesterhelt, D., and W. Marwan. 1987. Change of membrane potential is not a component of the photophobic transduction chain in *Halobacterium halobium*. *J. Bacteriol*. 169:3515–3520.
42. Marwan, W., W. Schäfer, and D. Oesterhelt. 1990. Signal transduction in *Halobacterium* depends on fumarate. *EMBO J*. 9:355–362.
43. Marwan, W., and D. Oesterhelt. 1991. Light-induced release of the switch factor during photophobic responses of *Halobacterium halobium*. *Naturwiss*. 78:127–129.
44. Montrone, M., W. Marwan, H. Grünberg, S. Musseleck, C. Starostzik, and D. Oesterhelt. 1993. Sensory rhodopsin-controlled release of the switch factor fumarate in *Halobacterium salinarium*. *Mol. Microbiol*. 10:1077–1085.
45. Barak, R., and M. Eisenbach. 1992. Fumarate or a fumarate metabolite restores switching ability to rotating flagella of bacterial envelopes. *J. Bacteriol*. 174:643–645.
46. Montrone, M., M. Eisenbach, D. Oesterhelt, and W. Marwan. 1998. Regulation of switching frequency and bias of the bacterial flagellar motor by CheY and fumarate. *J. Bacteriol*. 180:3375–3380.
47. Prasad, K., S. R. Caplan, and M. Eisenbach. 1998. Fumarate modulates bacterial flagellar rotation by lowering the free energy difference between the clockwise and counterclockwise states of the motor. *J. Mol. Biol*. 280:821–828.
48. Rudolph, J., and D. Oesterhelt. 1995. Chemotaxis and phototaxis require a CheA histidine kinase in the archaeon *Halobacterium salinarium*. *EMBO J*. 14:667–673.
49. Rudolph, J., N. Tolliday, C. Schmitt, S. C. Schuster, and D. Oesterhelt. 1995. Phosphorylation in halobacterial signal transduction. *EMBO J*. 14:4249–4257.
50. Hoff, W. D., K.-H. Jung, and J. L. Spudich. 1997. Molecular mechanism of photosignaling by archaeal sensory rhodopsins. *Annu. Rev. Biophys. Biomol. Struct*. 26:223–258.